Copyright © 1981, by the author(s).
All rights reserved.

Permission to make digital or hard copies of all or part of this work for personal or classroom use is granted without fee provided that copies are not made or distributed for profit or commercial advantage and that copies bear this notice and the full citation on the first page. To copy otherwise, to republish, to post on servers or to redistribute to lists, requires prior specific permission.

TWO-FREQUENCY FERMI MAPPING

by

J.E. Howard, A.J. Lichtenberg, and M.A. Lieberman

Memorandum No. UCB/ERL M81/86

28 August 1981

ELECTRONICS RESEARCH LABORATORY

College of Engineering
University of California, Berkeley
94720

TWO-FREQUENCY FERMI MAPPING

J.E. Howard, A.J. Lichtenberg, and M.A. Lieberman

Department of Electrical Engineering and Computer Sciences
and the Electronics Research Laboratory
University of California, Berkeley, California 94720

ABSTRACT

We examine the properties of the Fermi mapping with two driving terms,

$$u_{n+1} = u_n + \frac{\sin s\phi_n + \mu \sin r\phi_n}{\sqrt{1+\mu^2}}$$

$$\phi_{n+1} = \phi_n + \frac{4\pi M}{(r+s)u_{n+1}} \quad ,$$

where r and s are coprime integers, μ is the amplitude ratio of the driving terms, and M is a constant. Linear stability criteria and bifurcation thresholds are derived and confirmed numerically. Global stability limits are obtained by generalizing the criterion derived for the loss of stability of the last KAM surface between two neighboring island chains to the case of unequal size islands. The analytic estimates are compared with the numerical calculations and found to be in good agreement for $\mu \approx 1$. The results show that using two frequencies gives considerable destruction of local stability and an approximately twofold increase in energy (u^2) for the position of the lowest KAM barrier to stochastic heating.

Research sponsored by the Office of Naval Research under Contract N00014-79-C-0674 and by the Department of Energy Contract DE-ATOE-76ET53059.

1. INTRODUCTION

In this paper we study the effect of two driving frequencies on the stability properties of the Fermi mapping [1-2]. This two-dimensional area preserving mapping represents the motion of a light ball colliding elastically with a fixed and an oscillating wall, as depicted in Fig. 1. The case of a monochromatic sinusoidal wall velocity has been treated previously [3-6] and its stability properties are now well known. In such systems there exists a lowest (in velocity) invariant phase space curve that separates region of primarily regular motion from regions of connected stochasticity. A particle initially below such a Kolmogorov-Arnold-Moser (KAM) curve [7-8] cannot penetrate to higher velocities. As will be shown, the addition of a second wall frequency can significantly increase the velocity at which the first adiabatic barrier appears.

Adiabatic limits can be of practical importance in the cyclotron heating of plasmas in magnetic mirror devices [9]. The mapping method has been applied to electron cyclotron resonance heating (ECRH) by Jaeger et al. [10] and by Lieberman and Lichtenberg [11]. Ion cyclotron resonance heating (ICRH) has been similarly modelled by Howard and Kesner [12]. These treatments require that the particle-field interaction be sufficiently localized in order to justify an impulsive mapping model [13]. The theoretical results for ECRH have been verified experimentally for collisionless plasmas [14].

Recently it has been suggested that ECRH might be enhanced by using two or more closely-spaced frequencies, with the total RF power held fixed. Recent experiments by Lazar et al. [15] seem to substantiate this hope, although the precise reasons for the (approximately factor of two) increase in particle energy are not yet clear. Menyuk and Lee [16] have studied the effect of introducing a finite bandwidth of the driving frequency and found that all KAM curves could be effectively destroyed with a bandwidth equal to the orbital bounce frequency. However, this technique is difficult to realize experimentally.

Here we model the rather complex ECRH dynamics with the analogous, but far simpler Fermi model, as has previously been done for single frequency heating [5]. In order to produce a periodic mapping, we choose the two frequencies, ω_r and ω_s, in the ratio of some rational number $\omega_r/\omega_s = r/s$, where r and s are coprime integers. Taking r and s large, we can closely approximate any irrational number, or, with $r = s+1$, obtain closely spaced frequencies. Corresponding to each frequency we find sets of island chains which can overlap, thereby destroying nonlinear stability and increasing the adiabatic barrier.

In Section 2 we derive the basic mapping equations, and in Section 3 examine the linear stability of the island chains formed in the phase plane. Bifurcation thresholds follow naturally from the linear stability conditions. The principal results are contained in Section 4, where the nonlinear stability criterion [17] is extended to the case of unequal size islands. Numerical results are presented which substantiate both the linear and nonlinear stability criteria, and the bifurcation thresholds. Typically we find about a 50% increase in the adiabatic barrier velocity, corresponding to a twofold increase in kinetic energy, in qualitative agreement with experimental results on ECRH [15].

2. MAPPING EQUATIONS

The Fermi-Ulam model [1-2] consists of a light ball bouncing between a fixed and an oscillating wall, as illustrated in Fig. 1. In the simplified model [5], the oscillating wall transfers momentum to the ball instantaneously, without changing its position. The simplified model retains the essential features of the exact model [3,4] with the advantage of yielding an explicit area-preserving mapping.

Here we consider a momentum transfer having two frequency components normalized to maintain the sum of the amplitudes squared constant. (For uncorrelated sources, this gives constant input power.) The momentum change per collision is then

$$v_{n+1} - v_n = V_r \sin \omega_r t_n + V_s \sin(\omega_s t_n + \delta). \tag{1}$$

where $V_r^2 + V_s^2 = V^2 =$ constant.

The transit time between collisions with the moving wall is

$$t_{n+1} - t_n = \frac{2L}{v_{n+1}} , \tag{2}$$

where L is the wall separation and

$$\frac{\omega_r}{\omega_s} = \frac{r}{s} = p , \tag{3}$$

with r and s coprime integers. The phase δ does not have an appreciable effect on global stability and will be set equal to zero in what follows.

Defining the phase $\phi = \omega_s t/s$ and amplitude ratio $\mu = V_r/V_s$, (1) and (2) can be written in terms of the scaled velocity $u = v/V$ as

$$u_{n+1} = \left| u_n + \frac{\sin s\phi_n + \mu \sin r\phi_n}{\sqrt{1+\mu^2}} \right| \tag{4}$$

$$\phi_{n+1} = \phi_n + \frac{4\pi M}{(r+s)u_{n+1}} , \tag{5}$$

where the absolute value has been introduced in (4) to account for negative velocities. In deriving (5) we first symmetrized (2) in r and s by means of the identity

$$\frac{\omega_r}{r} = \frac{\omega_s}{s} = \frac{2\bar{\omega}}{r+s} , \qquad (6)$$

where

$$\bar{\omega} \equiv \frac{1}{2} (\omega_r + \omega_s) \qquad (7)$$

and then introduced the parameter

$$M \equiv L\bar{\omega}/V . \qquad (8)$$

Equations (4) and (5) constitute the desired normalized two-frequency mapping, fully symmetric in the integers r and s. It is straightforward to generalize them to include an arbitrary number of frequency components. In working with this mapping we shall fix L and $\bar{\omega}$ while varying r, s and μ. The limits $\mu = 0$ and ∞ yield simple Fermi-sine maps with known stability properties. It is the region $\mu \approx 1$, for which no nonlinear stability theory exists, that is of primary interest here. Although one usually requires $r \approx s$ in cyclotron heating applications, we are not limited by this restriction for the Fermi mapping.

Figure 2 shows a series of numerical surfaces of section (u vs. ϕ) for $r/s = 3/2$ and $M = 125$, and several values of μ. As usual, there are three distinct regions; a stochastic region at low velocities, an intermediate region with islands embedded in a stochastic sea, and a primarily regular region at higher velocities. Two critical velocities delimit these three zones: u_L, below which all period-one primary fixed points are unstable, and u_B, the adiabatic barrier, which bounds the region of connected stochasticity. For $\mu = 0$ there is a family of s-fold island chains at $u = 50$, 33.33, 25, etc., with smaller chains of secondary islands at the harmonics of ω_s. When $\mu > 0$ additional island chains associated with ω_r appear at $u = 37.5$, 30, etc. A secondary chain of five islands associated with $\omega_r + \omega_s$ can be clearly seen at $u \approx 41$ when $\mu = 1.0$. The linear stability limit, u_L, is seen to increase slowly with μ, while u_B makes large jumps at particular values of μ. When $\mu = 1$, the chains of primary islands at $u = 50$ and 25 have bifurcated from two to three islands, owing to the increasing influence of the ω_r driving term in (1). Theoretical expressions for the dependence of u_L and u_B on μ will be derived in Sections 3 and 4 and compared with numerical mappings in Section 4. Bifurcations are discussed briefly in Section 3 and in more detail in Ref. [20].

3. LINEAR STABILITY AND BIFURCATION OF PERIOD ONE FIXED POINTS

From (4) and (5), the period one ($\phi \rightarrow \phi + 2\pi k$) fixed points common to both frequencies are given by

$$u_{ok} = \frac{M_{eff}}{k}, \quad k = 1,2,3,\ldots \tag{9}$$

$$\sin s\,\phi_0 + \mu \sin r\phi_0 = 0, \tag{10}$$

where for convenience we have defined

$$M_{eff} = \frac{2M}{r+s}. \tag{11}$$

When $\mu = 0$ there exists an additional set of fixed points given by $s\phi \rightarrow s\phi + 2\pi k_s$, which includes the common set (9),

$$u_{os} = \frac{s\,M_{eff}}{k_s}, \quad k_s = 1,2,3,\ldots. \tag{12}$$

These fixed points have period P, where P/Q is s/k_s reduced to lowest terms. Similarly, when $\mu \rightarrow \infty$, setting $r\phi \rightarrow r\phi + 2\pi k_r$ yields period r fixed points at

$$u_{or} = \frac{r\,M_{eff}}{k_r}, \quad k_r = 1,2,3,\ldots \tag{13}$$

which also includes (9) as a subset. At intermediate values of μ the r- and s-fold islands at $\phi_0 = 0$ and π are unperturbed, but the other fixed points move according to (10), which locates the angular coordinate ϕ_0 independent of u_0. In general, (10) must be solved numerically for $\phi_0(\mu,r,s)$. $\phi_0 = 0, \pm\pi$ are obvious but not exhaustive solutions. We now investigate cases for which (10) may be solved analytically.

(a) $\mu \ll 1$. Regarding the μ term as a perturbation, the unperturbed solutions of (10) are

$$\phi_0 = 0, \pm\frac{\pi}{s}, \pm\frac{2\pi}{s}, \ldots, \pm\left(\frac{s-1}{s}\right)\pi, \pm\pi , \tag{14}$$

a total of 2s+1 roots in $[-\pi, \pi]$. Writing

$$F(\phi,\mu) = \sin s\phi + \mu \sin r\phi \approx F(\phi_0,\mu) + F'(\phi_0,\mu)(\phi - \phi_0) = 0 \tag{15}$$

then gives $\phi = \phi_0 - F_0/F_0'$, or

$$\phi(\mu) \approx \phi_0 - \frac{\mu \sin r\phi_0}{s \cos s\phi_0 + \mu r \cos r\phi_0} . \tag{16}$$

A similar application of Newton's method is of course possible in the limit $\mu \to \infty$.

(b) $\mu = 1$. For equal amplitudes (10) transforms to

$$\sin\left(\frac{r+s}{2}\right)\phi \quad \cos\left(\frac{r-s}{2}\right)\phi = 0 , \tag{17}$$

which yields the two families of solutions,

$$\phi_a = 0 , \frac{\pm 2\pi}{r+s} , \frac{\pm 4\pi}{r+s} , \ldots \tag{18}$$

$$\phi_b = \frac{\pm\pi}{r-s} , \frac{\pm 3\pi}{r-s} , \ldots . \tag{19}$$

There are a total of $1+[\frac{1}{2}(r+s)]$ ϕ_a roots, and $[\frac{1}{2}(r-s+1)]\,\phi_b$ roots, where [ ] denotes the integer part. In addition, there are several cases where (10) is exactly solvable for all μ, namely $r \leq 5$. We shall encounter these explicit solutions in the context of linear stability and bifurcation.

The linear stability theory of fixed points of arbitrary order is given in Ref. [5]. Here we calculate the stability limits of the primary period-one fixed points of the two-frequency Fermi mapping. As we shall see, these limits enable us to dilineate the bifurcations the primary island chains must make with increasing μ as they change from s-fold to r-fold symmetry.

Writing (4) and (5) in matrix form ,

$$\underset{\sim}{x}_{n+1} = T \cdot \underset{\sim}{x}_n \ , \tag{20}$$

with $\underset{\sim}{x} \equiv (u,\phi)$, the period-one primary fixed points are given by.

$$\underset{\sim}{x}_0 = T \cdot \underset{\sim}{x}_0 \ . \tag{21}$$

The stability in the neighborhood of x_0 is then determined by the linearized mapping,

$$\Delta\underset{\sim}{x}_{n+1} = \mathcal{L}\,\Delta\underset{\sim}{x}_n \ , \tag{22}$$

where $\mathcal{L}$ is the Jacobian matrix of T. The motion near x_0 is stable if and only if

$$|\mathrm{Tr}\mathcal{L}| < 2 \ . \tag{23}$$

From (4) and (5) we find

$$\mathrm{Tr}\mathcal{L} = 2 - \frac{4\pi M}{(p+1)\,u_0^2\sqrt{1+\mu^2}}\,(\cos s\phi_0 + \mu \cos r\phi_0) \ . \tag{24}$$

If $0 < \cos s\phi_0 + \mu \cos r\phi_0 < 1 + \mu p$, a sufficient stability condition is $\mathrm{Tr}\mathcal{L} > -2$, or

$$u_0^2 > u_L^2 = \frac{\pi M}{\sqrt{1+\mu^2}} \left(\frac{1+\mu p}{1+p}\right) \quad . \tag{25}$$

It should be noted that stable secondary fixed points, or higher period primary fixed points may exist below u_L. Also note that u_L has a maximum at $\mu = p$.

For $\mathrm{Tr}\mathcal{L} > 2$, a sufficient condition for instability is clearly

$$\cos s\phi_0 + \mu p \cos r\phi_0 < 0, \tag{26}$$

which is to be solved for μ and ϕ_0 simultaneously with (10). Since (26) is independent of u_0, we see that if $u_0 > u_L$, a stability threshold exists when

$$\cos s\phi_0 + \mu p \cos r\phi_0 = 0 \tag{27}$$

$$\sin s\phi_0 + \mu \sin r\phi_0 = 0 \ . \tag{10}$$

These equations admit a simple geometrical interpretation if we observe that they are of the form $F(\mu,\phi_0) = \partial F/\partial\phi_0 = 0$. As this is just the condition for a double root of (10), it follows that (10) and (27) together determine the bifurcations of the common fixed points as the mapping changes (with increasing μ) from s-fold to r-fold symmetry. That is, for fixed r and s, one or more common fixed points ϕ_0^* bifurcate at critical values μ^*.

In general there are three types of bifurcation; the pitchfork bifurcation (P) in which a stable fixed point destablizes and gives birth to two nearby stable fixed points; the anti-pitchfork bifurcation ($P^\dagger$) in which an unstable fixed point stablizes and issues forth two unstable fixed points; and lastly, the tangent bifurcation (T), in which a stable-unstable pair of fixed points is created.

Although all this information is in principle contained in (10) alone, (27) is often useful in practice. For example, (10) yields the immediate fixed points $\phi_0 = 0, \pi$. Equation (27) gives $1 + \mu p = 0$ for $\phi_0 = 0$ and we conclude that this point never bifurcates for $u > u_L$. For $\phi_0 = \pi$, however, (27) yields $(-1)^s + \mu^* p(-1)^r = 0$, which has the solution $\mu^* = 1/p$, provided that r-s is odd. In particular, if r-s = 1, this is the only bifurcation, giving birth to two new fixed points, exactly the required number to change from s-fold to (s+1)-fold symmetry. This bifurcation is clearly seen in Fig. 2d.

Another broad class of bifurcations is revealed by setting $\phi_0 = \pm \frac{\pi}{2}$ in (10) and (27). Setting $r = s+2m$, $m = 1,2,3,\ldots$, (27) is satisfied, since r and s must be odd in order to be coprime. Equation (10) becomes $1 + \mu \cos \pi m = 0$, which is satisfied by $\mu^* = 1$ and m odd. Thus, a pair of tangent bifurcations occurs at $\phi_0^* = \pm \pi/2$ when $\mu^* = 1$ for $r = s+2, s+6, \ldots$. Again, when $r-s = 2$, these are the only possible bifurcations.

For $s < r \leq 5$, complete algebraic solutions of (10) and (27) may be obtained by means of the factorization

$$\sin n\phi = \sin\phi \, P_{n-1} (\cos \phi) , \qquad (28)$$

where $P_{n-1}(\cos \phi)$ is a polynomial of degree n-1. Thus, (10) becomes

$$P_{s-1}(\cos \phi) + \mu P_{r-1}(\cos \phi) = 0 . \qquad (29)$$

The critical values of μ are then given by the vanishing of the discriminant of (29), except in a few degenerate cases. The bifurcation angle ϕ_0^* usually follows by inspection or, if necessary, by numerical solution of (10). The calculated values of ϕ_0^* and μ^* and the bifurcation type are listed in Table 1. Formal solutions of (29) are given in Ref. [20].

Additional insight into the structure of the bifurcation may be gleaned from the averaged Hamiltonian (derived in the next section)

$$\hat{H} = \frac{1}{2} G\, u^2 + V(\phi) \; , \tag{30}$$

where G is a constant and, for a common island chain,

$$V(\phi) = -\frac{1}{\sqrt{1+\mu^2}} \left(\frac{1}{s} \cos s\phi + \frac{\mu}{r} \cos r\phi \right) \tag{31}$$

is the effective potential. At a pitchfork or antipitchfork bifurcation, $V' = V'' = V''' = 0$, while $V''' \neq 0$ for a tangent bifurcation. Thus, tangent bifurcations arise from inflection points in $V(\phi)$, while pitchfork bifurcations stem from third order critical points. More exotic bifurcations may be produced from potentials having higher order singular points [19]. A set of calculated level curves and their associated effective potentials are shown in Fig. 3 for the case $r/s = 3/2$. Note the pitchfork bifurcation at $\phi = 180°$ when $\mu = 2/3$, as predicted.

4. NONLINEAR STABILITY AND GLOBAL STOCHASTICITY

4.1 Derivation of Averaged Equations

In order to determine the limit to particle heating from below, it suffices to find the lowest velocity for which a KAM curve spans the entire range of phases. This global stochasticity limit has been calculated for the single frequency Fermi map [5] and in detail for the Chirikov-Taylor "standard map" [17,18], which locally approximates the Fermi map. The destruction of KAM curves may be understood intuitively as arising from the interaction of neighboring island chains. Each island possesses a stochastic layer about its separatrix, so that for sufficiently large island widths these layers overlap, permitting diffusion over the region of velocity space occupied by the two islands.

The island width is easily calculated from an approximate Hamiltonian in which only the dominant resonant term is retained, with all other terms averaged out. Analytic and numerical calculations show that the last KAM curve lying between two contiguous islands is destroyed when the sum of the island half-widths equals approximately two-thirds the distance between the island centers measured in action space (velocity in our problem). This criterion has been shown to be quite sharp for equal-width islands [18] and works reasonably well if the widths are not too disparate [5]. Escande and Doveil [21] have derived a criterion valid for two islands with unequal widths, but their method is difficult to apply owing to the influence of neighboring large islands. We therefore employ here the simpler "two-thirds rule," which agrees well with numerical calculations for comparable-sized islands.

We begin by defining slowly changing variables near the s-fold elliptic fixed points,

$$u_s = u - u_{os} \qquad (32)$$

$$\hat{\theta}_s = \theta - \theta_{os} ,$$

where $\theta = s\phi$ and

$$u_{os} = sM_{eff}/k_s$$

$$\theta_{os} = 2\pi k_s n , \qquad (33)$$

with n the iteration number of the mapping. For $\mu \neq 0$ only the fixed points at $\theta_{os} = 0$ and π are unperturbed. Neglecting the perturbation of the other fixed points, the mapping (4)-(5) in the vicinity of the s-fold chain may be written in terms of n as

$$\frac{d\hat{u}_s}{dn} = \frac{\sin\theta + \mu \sin\left(\frac{r\theta}{s}\right)}{\sqrt{1+\mu^2}} \sum_{n=-\infty}^{\infty} \delta(n-m) \qquad (34)$$

$$\frac{d\theta_s}{dn} = -\frac{2\pi s\, M_{eff}}{u_{os}^2} u_s \,,$$

where (5) has been expanded about u_{os}. (35)

Fourier expanding the train of delta functions

$$\sum_{m=-\infty}^{\infty} \delta(n-m) = \sum_{\ell=-\infty}^{\infty} e^{2\pi i \ell n} \tag{36}$$

and averaging (34) over n, we find that the first term survives for $\ell = \pm k_s$, while the second term is slowly varying only if $\ell \approx \pm\, rk_s/s$, which is only true near the common fixed points, not considered here. Thus, the averaged form of (34) is simply

$$\frac{du_s}{dn} = \frac{\sin \hat{\theta}_s}{\sqrt{1+\mu^2}} \;. \tag{37}$$

Equations (35) and (37) are derivable from the averaged Hamiltonian

$$\hat{H}_s = \frac{2\pi s\, M_{eff}}{u_{os}^2} \frac{\hat{u}_s^2}{2} - \frac{\cos \hat{\theta}_s}{\sqrt{1+\mu^2}} \;, \tag{38}$$

which yields the island amplitude

$$\Delta_s = (1+\mu^2)^{-1/4} \left(\frac{2\, u_{os}^2}{\pi s\, M_{eff}} \right)^{1/2} \;. \tag{39}$$

Similarly, expanding u and θ about an r-fold chain gives

$$\Delta_r = \sqrt{\mu} \quad (1+\mu^2)^{-1/4} \left(\frac{2u_{or}^2}{\pi r\, M_{eff}} \right)^{1/2} \;. \tag{40}$$

Equations (39) and (40) are generally valid only for $\mu \ll 1$ and $\mu \gg 1$, respectively, when the fixed points are well approximated by (10). Nevertheless, a useful overlap criterion may be obtained by focusing on the $\theta_{os} = 0$ (mod 2π) fixed point, which is unperturbed for all μ and elliptic for $u > u_L$. The widths Δ_r and Δ_s are valid for these central islands for arbitrary μ.

The motion near the common fixed points is obtained in the same manner by keeping the terms in the δ-function satisfying $\ell = \pm k_s$ and $\ell = \pm\, rk_s/s$, simultaneously:

$$\frac{d\hat{u}}{dn} = \frac{\sin s\hat{\phi} + \mu \sin r\hat{\phi}}{\sqrt{1+\mu^2}} \tag{41}$$

$$\frac{d\hat{\phi}}{dn} = -\frac{2\pi M_{eff}}{u_o^2}\,\hat{u} \quad . \tag{42}$$

Integrating these equations then gives the averaged Hamiltonian for the common fixed points,

$$\hat{H} = \frac{1}{2} G\hat{u}^2 - \frac{1}{\sqrt{1+\mu^2}} \left(\frac{1}{s} \cos s\phi + \frac{\mu}{r} \cos r\phi \right) \quad , \tag{43}$$

where

$$G = \frac{2\pi M_{eff}}{u_o^2} \quad . \tag{44}$$

Calculation of the island width in this case is complicated by the sequence of bifurcations as μ increases from 0 to ∞. As discussed in Section 3, this calculation can be carried out explicitly only for the particular values of r and s listed in Table 1. A width can be calculated explicitly for the central island at $\phi_0 = 0$, which is elliptic for all μ. For $\mu \ll 1$ a single separatrix crosses the $u = u_o$ line at $\phi_c = \pm\, \pi/s$ (mod 2π), but at larger μ there is in general a complex system of nested separatrices, the outermost of which first overlaps with the separatrices of neighboring island chains.

In terms of the angle ϕ_c the central island width is given by

$$\Delta^2 = \frac{4}{G\sqrt{1+\mu^2}} \left[\frac{1}{s} \sin^2 \left(\frac{s\phi_c}{2}\right) + \frac{\mu}{r} \sin^2 \left(\frac{r\phi_c}{2}\right) \right] \quad . \tag{45}$$

Taking $r/s = 3/2$ as an example we find

$$\Delta^2 = \frac{8\mu^3 + 18\mu^2 + (1+4\mu^2)^{3/2} - 1}{12\, G\, \mu^2 \sqrt{1+\mu^2}} \quad , \tag{46}$$

which varies by only 30% as μ varies from 0 to ∞ and by only 2% in the range $0 < \mu < 1$.

In general, for $r > s, \Delta(\mu)$ is either monotonic decreasing or has a gentle maximum near $\mu = 0.5$. In all cases (45) gives

$$\frac{\Delta(0)}{\Delta(\infty)} = \sqrt{\frac{r}{s}} \ . \tag{47}$$

Thus, for closely spaced frequencies the variation of $\Delta(\mu)$ is entirely negligible, so that we may take

$$\Delta \approx \Delta(0) = \frac{2}{\sqrt{Gs}} \ . \tag{48}$$

In extreme cases one must calculate the angle ϕ_c and use (45); for $\mu = 1$ one may easily obtain ϕ_c from (18). More information on island widths may be found in Ref. [20].

4.2 Overlap Criterion

Having outlined a procedure for calculating approximate island widths, we now turn to the choice of an appropriate overlap criterion for estimating the loss of global stability with increasing μ. A useful rule of thumb is the "two-thirds rule" [18],

$$\Delta_1 + \Delta_2 > \frac{2}{3} |u_{o1} - u_{o2}| \ , \tag{49}$$

where u_{o1} and u_{o2} are the two resonance positions and Δ_1 and Δ_2 are the resonance half-widths Δ_r, Δ_s or Δ, as the case may be. In deriving (49) it is implicitly assumed that the islands are of comparable size, so that the secondary islands are smaller than the primary islands and the level curves of one island chain are not significantly distorted by the level curves of the other. Thus, in applying (49) to the two-frequency Fermi mapping, we expect good agreement for $\mu \approx 1$ but only qualitative predictions for $\mu \ll 1$ or $\mu \gg 1$. In the latter cases, although (49) still predicts KAM destruction quite accurately, the precise value of μ at which this occurs is predicted less accurately, μ (or μ^{-1}) being a perturbation.

We consider three controlled numerical experiments in examining the effect of two frequencies on stochasticity. In the first, M is held fixed, while μ is varied from 0 to ∞. As μ is "turned on," the r-fold islands grow rapidly and interact with s-fold and common islands, large jumps in the adiabatic barrier u_B generally occurring at fairly small values of μ. In the second numerical experiment, we hold μ fixed and vary M. Here (49) will be seen to give accurate predictions of the jump in the adiabatic barrier. In the third experiment we hold M and μ fixed and vary the frequency ratio r/s.

Of the several possible combinations of overlapping r-fold, s-fold and common islands, we choose for illustration only two. For overlap of the k_s and k_s+1 fold chains, using (9), (11), and (48) in (49) gives $M < M^*$, with

$$M^* = \frac{9}{4\pi} \left(\frac{r+s}{s}\right) (2k_s+1)^2 \sqrt{1+\mu^2} \quad , \tag{50}$$

which is equivalent to the single frequency overlap criteria for $\mu \ll 1$. For overlap of an r and as s-fold chain, using (12), (13) (39) and (40) in (49) yields

$$M^* = \frac{9}{4\pi} \left(\frac{r+s}{s}\right) \left[\frac{1 + \frac{k_s}{k_r}\sqrt{\frac{\mu r}{s}}}{1 - \frac{rk_s}{sk_r}} \right]^2 \sqrt{1+\mu^2} \quad . \tag{51}$$

However, care must be exercised in using this result for μ very small, as overlap is then determined by neighboring s-chains and their perturbation by interspersed r-chains.

The use of the criterion (49) (and its limitations) are best illustrated by an example. We first fix $r/s = 3/2$ and $M = 125$, and consider the effect of varying μ. The mapping for $\mu = 0$ is shown in Fig. 2(a), which also shows the locations of the island chains as given by (9), (11) and (13) for several values of k, k_r and k_s. The $k_s = 2$-8 islands are clearly visible, but the $k_s = 9$ chain ($u_0 = 11.1$) falls beneath the linear stability limit and has disappeared. Numerically, we find the last KAM curve at about $u_B = 27$, as indicated in the figure, in agreement with the overlap criterion (50), which predicts that KAM surfaces exist between the $k_s = 3$ and 4 island chains, but not between the $k_s = 4$ and 5 chains.

As we increase μ to 0.1, the adiabatic barrier increases dramatically to $u_B = 37$. This jump is due to the intercession of the $k_r = 5$ islands at $u_{0r} = 30$, whose stochastic layer overlaps those of the $k_s = 3$ and 4 islands at $u_{0s} = 33.33$ and 25. Applying the overlap criterion, we find that the $k_s = 3$ and $k_r = 5$ islands overlap for arbitrarily small μ, but that overlap of the $k_r = 5$ and $k_s = 4$ islands should not occur until $\mu > 0.5$. The underlying reason for this premature overlap is the chain of four secondary islands at $u_0 \approx 28$, which may be seen in Fig. 2(b). There is also a chain of six secondary islands at $u_0 \approx 27$, barely visible in Fig. 2(b). These two secondary chains effectively bridge the gap between the $k_r = 5$ and $k_s = 4$ islands, so that overlap occurs at $\mu \approx .065$.

As μ is increased from 0.1 to 0.25, u_B once again suddenly increases, as the $k_r = 4$ islands at $u_{0r} = 37.5$ grow and overlap with the $k_s = 3$ islands at $u_{0s} = 33.33$. According to theory this jump should occur at $\mu = 0.0025$, whereas it does not actually occur until $\mu = 0.15$. The underlying reason for this discrepancy is the great difference in size of the two islands, the smaller being distorted with no significant intermediate island chain to mediate the overlap. To complete this series of $r/s = 3/2$ cases we include the mapping for $\mu = 1$. Here the two-thirds rule successfully predicts that the $k = 1$ chain at $u_0 = 50$ cannot overlap the $k_r = 4$ chain at 37.5. (Note that the common island chain at $u_0 = 50$ has bifurcated at $\phi = 180°$ and that the r-fold chain at $u_{or} = 37.5$ has undergone a more complex division (trifurcation) into three islands.) The observed variation of u_B with μ is shown in Fig. 4. The inability of the two-thirds rule to predict the exact value of μ at which two island chains overlap, for small μ, is not surprising. Since μ enters the overlap condition in (51) as a perturbation, a significant change in μ corresponds to only a small change in the overlap criterion itself.

For $\mu \approx 1$ we expect much better agreement, which is in fact found numerically. To illustrate this, Fig. 5 presents u_B as a function of M for $\mu = 0$ and 1 (Eq. (49) is always solvable for M). To follow a given KAM curve with changing M, we note that in the absence of overlap, the island centers, and therefore u_B, are proportional to M. However, the island width $\Delta \sim \sqrt{M}$, so that an overlap must inevitably occur for a given island chain as M is decreased, with the chain continuing to sink into the stochastic sea as M decreases further. For $\mu = 0$ we follow only the s-fold islands, while for $\mu = 1$ we must examine all possible combinations of r-fold, s-fold and common islands. The solid zig-zag curves represent the theoretical formula (49), with the numerical results shown as individual points. The dashed line indicates the average proportionality

$u_B \sim \sqrt{M}$. The agreement between theory and numerical values is seen to be quite good.

We have also examined a number of other cases, varying the value of r and s to determine first if the two-thirds rule for overlap holds and also to investigate the fractional jump in the action as r and s become larger. Specifically, we take $r = s+1$ and consider $s = 1,2,3,4,\ldots$. For fixed M, this corresponds to taking the two frequencies successively closer together. Of particular interest here is the case $s = 1$, both theoretically because of the simplicity of the interspersed island structure, and practically because a second harmonic may be generated naturally in a physical system. Because the r-fold islands are interspersed halfway between the s-fold chains and reinforce the second harmonics of the s symmetry, we might expect particularly good agreement with the two thirds overlap criteria. This is indeed the case as seen in Fig. 6, which graphs u_B against μ for $r/s = 2/1$. The arrow at $\mu = 0.39$ indicates the predicted overlap of the $k_r = 3$ and $k_s = 2$ island chains, in excellent agreement with the value of $\mu = 0.35$ at which the last KAM surface between these islands disappears. The smaller jumps in the adiabatic barrier between these two major chains involve the interaction of secondary islands and are therefore not predicted by the first order theory.

Generally the theory predicts whether, for given μ, the last KAM surface between any two island chains is destroyed. To demonstrate this, we calculate the maximum change in u_B over a large range of μ, for $r = s+1$ and fixed M. The results are shown in Fig. 7, which plots the relative change in u_B,

$$\eta = \frac{u_B(1) - u_B(0)}{u_B(0)} \qquad (52)$$

as a function of 1/s, where $u_B(1) \equiv u_B(\mu=1) \approx u_{Bmax}$.

For large $s(1/s < 0.05)$ the r-fold and s-fold islands nearly coincide near u_B, so that we would expect no increase in u_B with increasing μ. However, as Fig. 7 shows, the calculated change decreases at first with increasing s, but does not fall to zero as expected. This residual change is apparently due to the mutual destruction of closely spaced r-fold and s-fold island chains and a small increase in island width due to the normalization. The oscillations in η at smaller s can be understood in terms of the resonance interspersal, the maxima occurring when the resonances are evenly spaced near the adiabatic barrier. From the fixed point conditions (12) and (13) the r-fold and s-fold islands are evenly interspersed where

$$\frac{2rM_{eff}}{k_r} = \frac{sM_{eff}}{k_s} + \frac{sM_{eff}}{k_{s+1}} \quad . \tag{53}$$

Taking $r = s+1$ and $k_r = k_s + m$ then gives, for $k_s >> 1$,

$$k_s = \frac{1}{2}(2m-1)s, \tag{54}$$

which implies $s >> 1$ for moderate m.

If we evaluate u_{os} at the adiabatic barrier $u \; = \alpha \sqrt{2\pi M}$, where $M_{eff} \cong M/s$ and α is approximately equal to the increase in u_B due to two frequencies, then (55) becomes

$$\frac{1}{s} = \alpha(2m-1)\sqrt{\frac{\pi}{2M}} \quad . \tag{55}$$

The maximum enhancement thus occurs at a set of odd integer values, $m' = 2m-1$. Conversely, the s and r resonances are centered on top of one another for even integers $m' = 2m$, where we expect η to be a minimum, i.e,

$$\frac{1}{s} = \alpha 2m\sqrt{\frac{\pi}{2M}} \quad . \tag{56}$$

From these results and the position of the s and r island chains from (12) and (13), we expect the last KAM curves to be destroyed at $\alpha = 1.4$ to give the peaks, and at $\alpha = 1.1$ to give the minimum. These values of 1/s are shown on Fig. 7 as arrows, which indicate reasonable agreement with the predictions of (55) and (56).

5. DISCUSSION

The addition of a second driving frequency to the Fermi mapping produces a considerable enrichment of the phase plane structure. This can be seen, for example, by comparison of Figs. 2a and 2d. A new set of islands appear, corresponding to the fixed points of the second frequency. The islands associated with the fixed points common to both frequencies become considerably more involved, with bifurcations changing the island topology. Stochasticity near the separatrices of the bifurcated islands decreases the area occupied by local KAM curves (islands). Interactions also occur between the lowest order islands of one symmetry and higher order islands of the second symmetry, giving rise to very interesting island structures.

The addition of a second set of islands, with their own stochastic layers interpersed among the first set of islands, leads to an interaction which destroys the KAM surfaces between islands at lower driving amplitude. The two-thirds rule, which was developed to predict when the last KAM surface between neighboring equal width island chains is destroyed, is applied to the two-frequency Fermi map with its islands of unequal width. It is found that the rule works well unless the islands are very different in size. Comparing the results of Figs. 2a and 2d it is seen that the last adiabatic barrier increases from the single-frequency value $u_B = 27$, above the $k_s = 4$ island centered at $u = 25$, to $u_B = 37$, above the $k_s = 3$ island centered at $u = 33.3$. These results are in agreement with the two-thirds rule.

Considering the Fermi acceleration model as an analog to electron cyclotron resonance heating, our results have implications for the heating problem. If the resonances are fairly evenly interspersed near the adiabatic barrier, then for a given input power it is possible to increase the energy obtained by stochastic heating by a factor of two, by employing two heating frequencies rather than one.

We can also relate the requirement for interspersed resonances found for the Fermi acceleration model to ECRH. From the definition of phase slip $s\Delta\phi$ in (5) we see that

$$\frac{sM_{eff}}{u_{os}} = \frac{\omega_s}{2\omega_B} \quad , \tag{57}$$

where $\omega_B = \pi u/\ell$ is the "bounce frequency" corresponding to two mapping periods and ω_s is the driving frequency. Substituting M_{eff}/u_{os} from (12) into (57) and noting that $\delta\omega = \omega_r - \omega_s = \omega_s/s$, we have for interspersed resonances

$$\delta\omega = (2m-1)\omega_B . \tag{58}$$

This result is consistent with a numerical calculation by Rognlien [22], which indicates peaks in the ECRH induced heating rate for frequency separations satisfying (58). A peak in ECRH heating was also found experimentally to occur when $\delta\omega = \omega_B$ [15].

There are additional constraints that must be satisfied in an ECRH experiment, such as the spatial overlap of the heating zones of the two frequencies, which do not arise in the present study. The ECRH problem also has additional degrees of freedom which can lead to quite different phenomena, such as Arnold diffusion [23]. These considerations of both theoretical and practical importance leave considerable scope for future work on this problem.

References

[1] E. Fermi, Phys. Rev. 15(1949) 1169.

[2] S. Ulam, Proc. 4th Berkeley Symp. on Math. Stat. and Prob. 3 (Univ. of Calif. Press, 1961), p. 315.

[3] G. M. Zaslavskii and B. V. Chirikov, Soviet Physics Doklady 9(1965) 989.

[4] A. Brahic, Astr. and Astrophys. 12(1971) 98.

[5] M. A. Lieberman and A. J. Lichtenberg, Phys. Rev. A5(1972) 1852.

[6] A. J. Lichtenberg, M. A. Lieberman and R. H. Cohen, Physica D (1980) 291.

[7] V. I. Arnold, Russian Math. Survey 18(1963) 9.

[8] J. Moser, Stable and Random Motions in Dynamical Systems, Ann. of Math. 77 (Princeton Univ. Press, Princeton, N.J., 1973).

[9] T.H. Stix, Nucl. Fusion 15(1975) 737.

[10] E. F. Jaeger, A. J. Lichtenberg and M. A. Lieberman, Plasma Phys. 14(1972) 1073.

[11] M. A. Lieberman and A. J. Lichtenberg, Plasma Phys. 15(1973) 125.

[12] J. E. Howard and J. Kesner, "ICRF Heating in a Tandem Minor," Univ. of Wisconsin Nuclear Engineering Report UWFDM-280, 1979.

[13] J. E. Howard, Plasma Phys. 23(1981) 597.

[14] N. C. Wyeth, A. J. Lichtenberg and M. A. Lieberman, Plasma Phys. 17 (1975) 679.

[15] B. H. Quon et al., Bull. Am. Phys. Soc. 26(1981) 893.

[16] C. R. Menyuk and Y. C. Lee, Phys. Fluids 23 (1980) 2225.

[17] B. V. Chirikov, Physics Reports 52(1979) 263.

[18] A. J. Lichtenberg, in Intrinsic Stochasticity in Plasmas, C. Laval and D. Gresillon, Ed., Editions de Physique, Orsay (1979) 13.

[19] I. Stewart, Physica D 2(1981) 245.

[20] J. E. Howard, M. A. Lieberman and A. J. Lichtenberg, "Bifurcations of the Two-Frequency Fermi Map," UCB/ERL Memorandum M81/56 (1981), University of California, Electronics Research Lab.

[21] D. F. Escande and F. Doveil, Physics Lett. 83A(1981) 307.

[22] T. D. Rognlien, Bull. Am. Phys. Soc. 26, 1035 (1981).

[23] J. L. Tennyson, M. A. Lieberman and A. J. Lichtenberg, AIP Conf. Proc. No. 57, Nonlinear Dynamics and the Beam-Beam Interaction, M. Month and J. C. Herrera, Eds., (1979) 272.

TABLE 1

r/s	ϕ_0	μ^*	Type
2/1	180°	1/2	$P^\dagger$
3/1	90°	1	T
3/2	180°	2/3	P
4/1	180°	1/4	$P^\dagger$
	65.91°	$3\sqrt{6}/8$	T
4/3	180°	3/4	$P^\dagger$
5/1	52.24°	4/5	T
	127.76°		T
5/2	180°	2/5	P
	55.80°	0.9414	T
5/3	90°	1	T
5/4	180°	4/5	P
(n+1)/n	180°	n/(n+1)	P or $P^\dagger$
(n+2)/n	90°	1	T

FIGURE CAPTIONS

Fig. 1. The Fermi model. A light ball of velocity u makes elastic collisions with a fixed wall and an oscillating wall, separated by the average distance L.

Fig. 2. Surfaces of section for $r/s = 3/2$, $M = 125$ and four values of μ. The locations of several common, rfold and sfold island chains are given in the first plot. The linear stability limit u_L and adiabatic barrier u_B are indicated in each case.

Fig. 3. Theoretical level curves and effective potential for $r/s = 3/2$ and four values of μ. Note the pitchfork bifurcation of the elliptic fixed point at $\phi = \pi$ when $\mu = 2/3$, and the corresponding change in $V(\phi)$.

Fig. 4. Adiabatic barrier as a function of μ for $r/s = 3/2$ and $M = 125$. The jumps in u_B are associated with overlap of the island chains indicated in the right hand margin.

Fig. 5. Adiabatic barrier as a function of M for $\mu = 0$ and 1. The solid "zig-zag" curves were calculated using the two-thirds rule, while the circles were obtained by numerically iterating the mapping 10^6 times.

Fig. 6. Adiabatic barrier as a function of μ for $r/s = 2/1$ and $M = 50$. The agreement between the theory and the numerical data is much better in this case, since the jumps occur at larger μ.

Fig. 7. Fractional increase in u_B as a function of $1/s$ for $M = 500$. According to theory the increase should vanish for $s \gtrsim 100$. The residual change is probably due to the strong interaction of overlapping r- and sfold island chains.

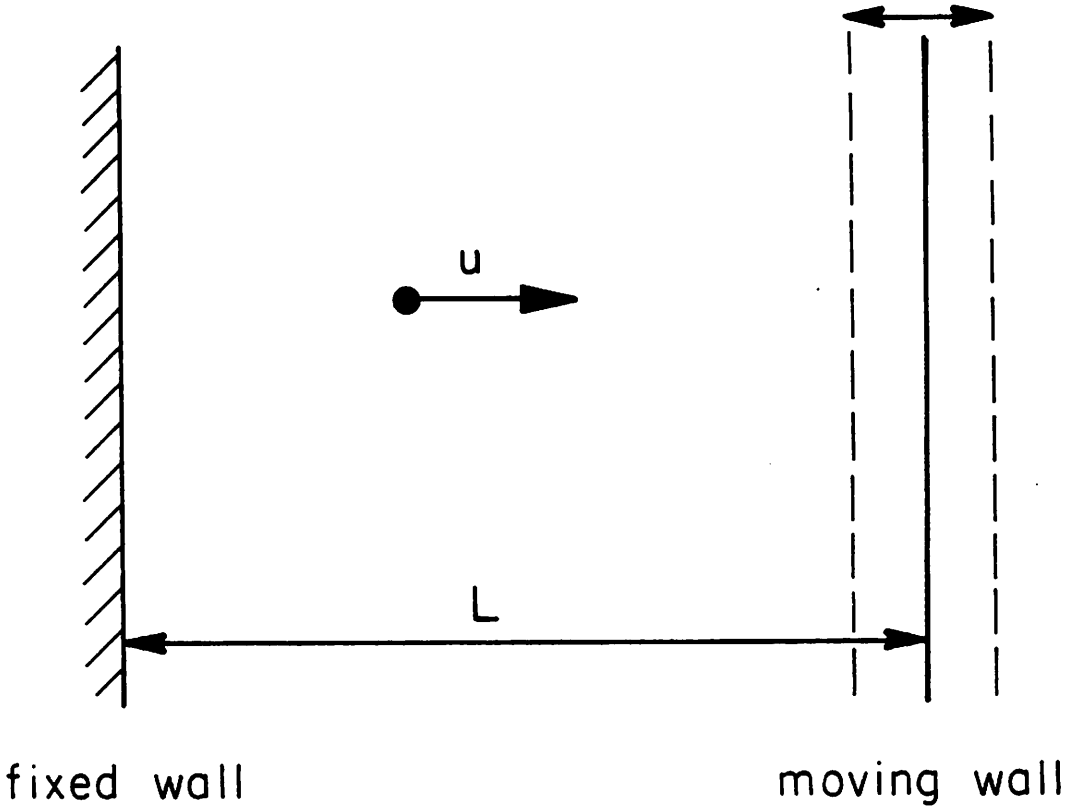
u
L
fixed wall
moving wall

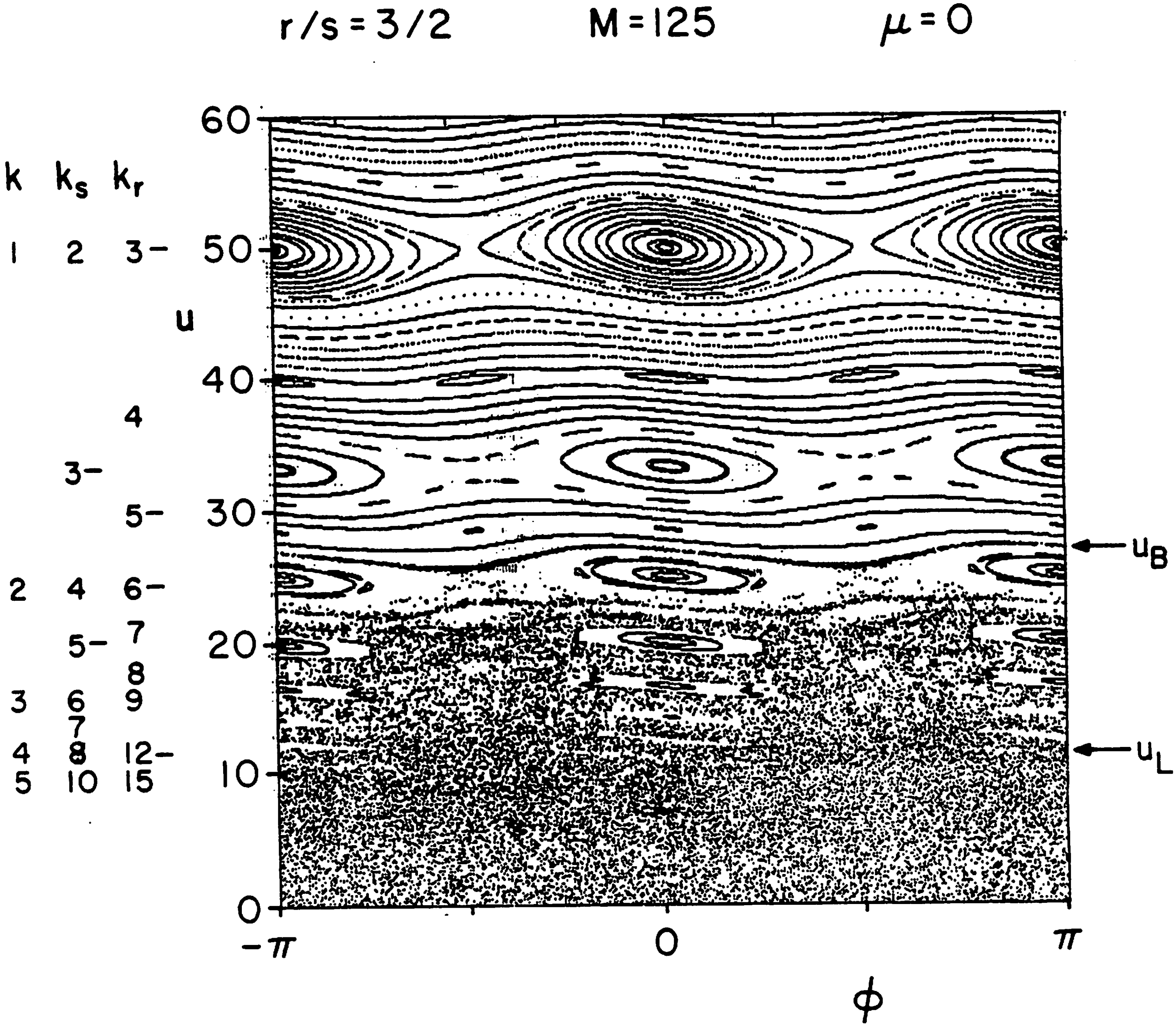
r/s = 3/2 M = 125 μ = 0
k k_s k_r
1 2 3–
4
3–
5–
2 4 6–
5– 7
8
3 6 9
7
4 8 12–
5 10 15
u
60
50
40
30
20
10
0
u_B
u_L
–π
0
π
φ

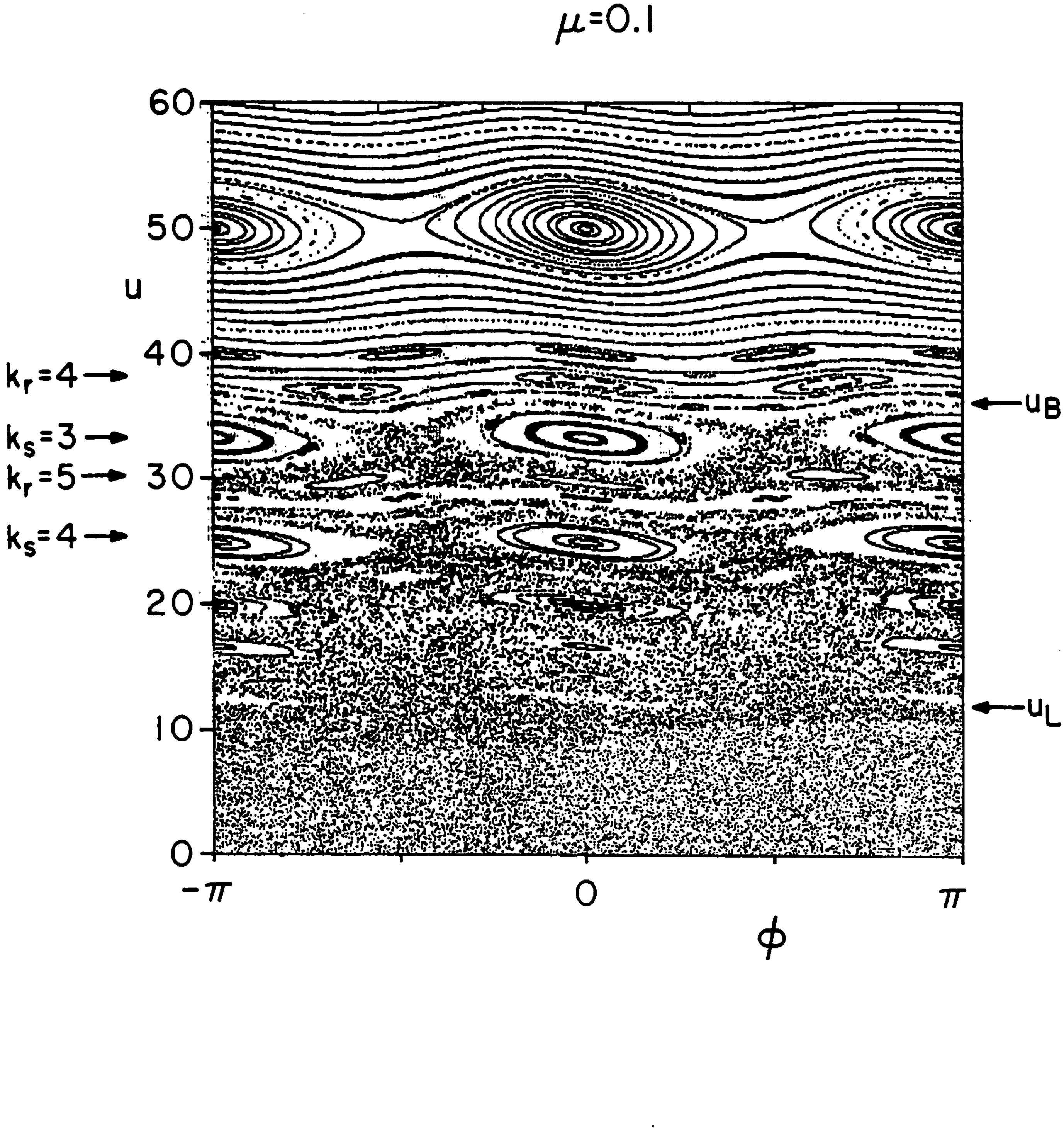
μ=0.1
60
50
40
30
20
10
0
u
k_r=4
k_s=3
k_r=5
k_s=4
u_B
u_L
−π
0
π
φ

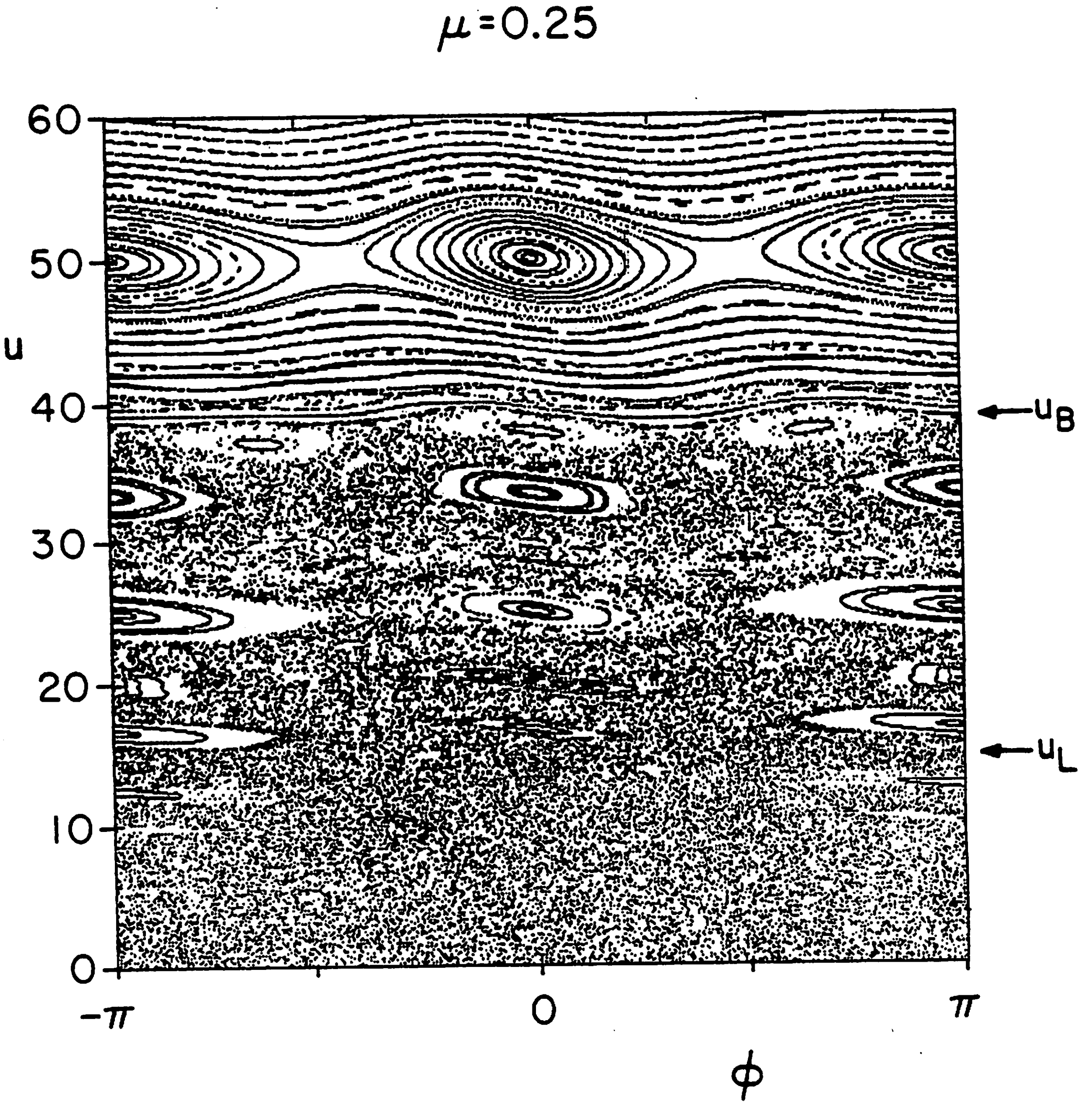
μ=0.25
60
50
u
40
30
20
10
0
−π
0
π
ϕ
u_B
u_L

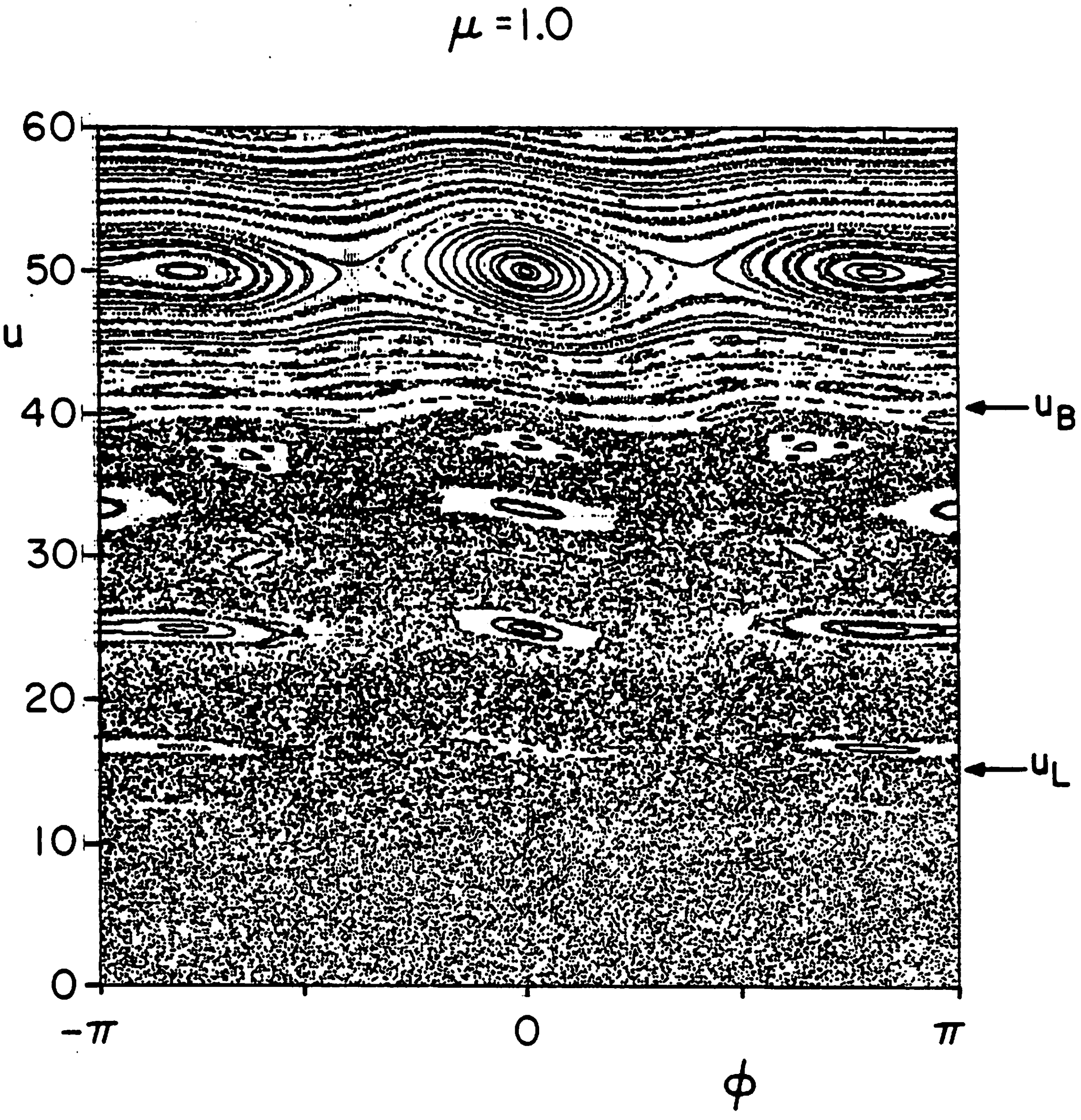
$\mu = 1.0$
60
50
40
30
20
10
0
u
u_B
u_L
$-\pi$
0
π
ϕ

r/s=3/2

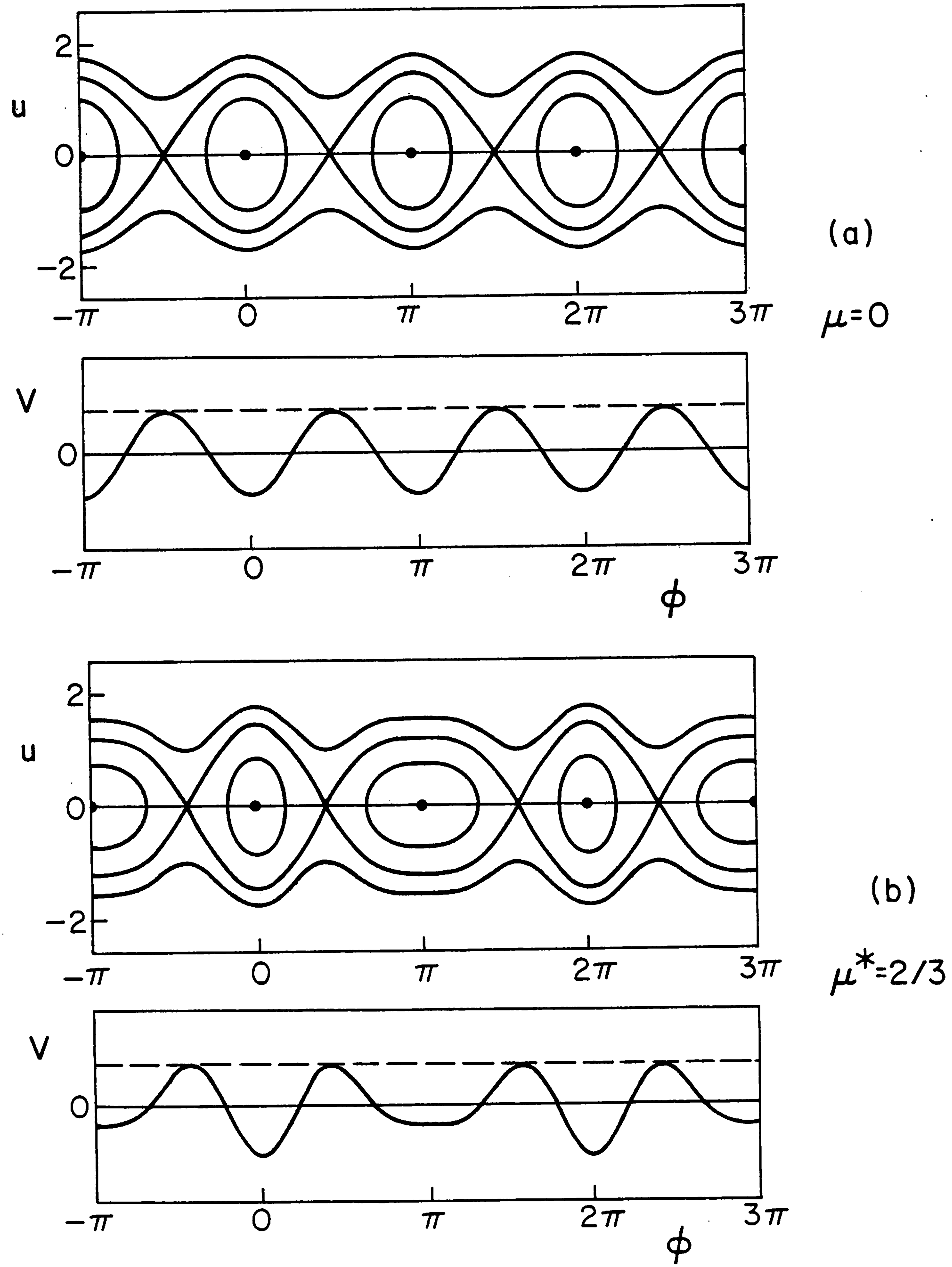

r/s = 3/2

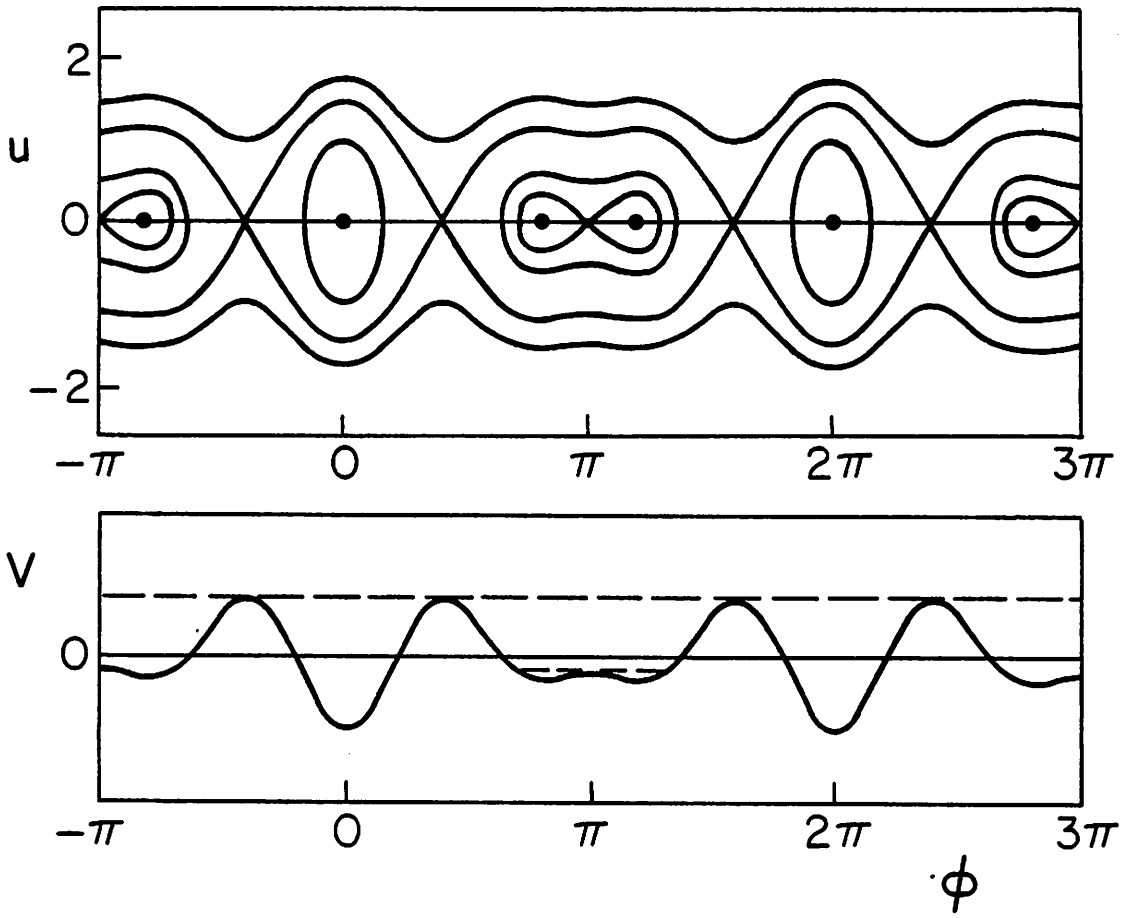

(c)

μ = 1

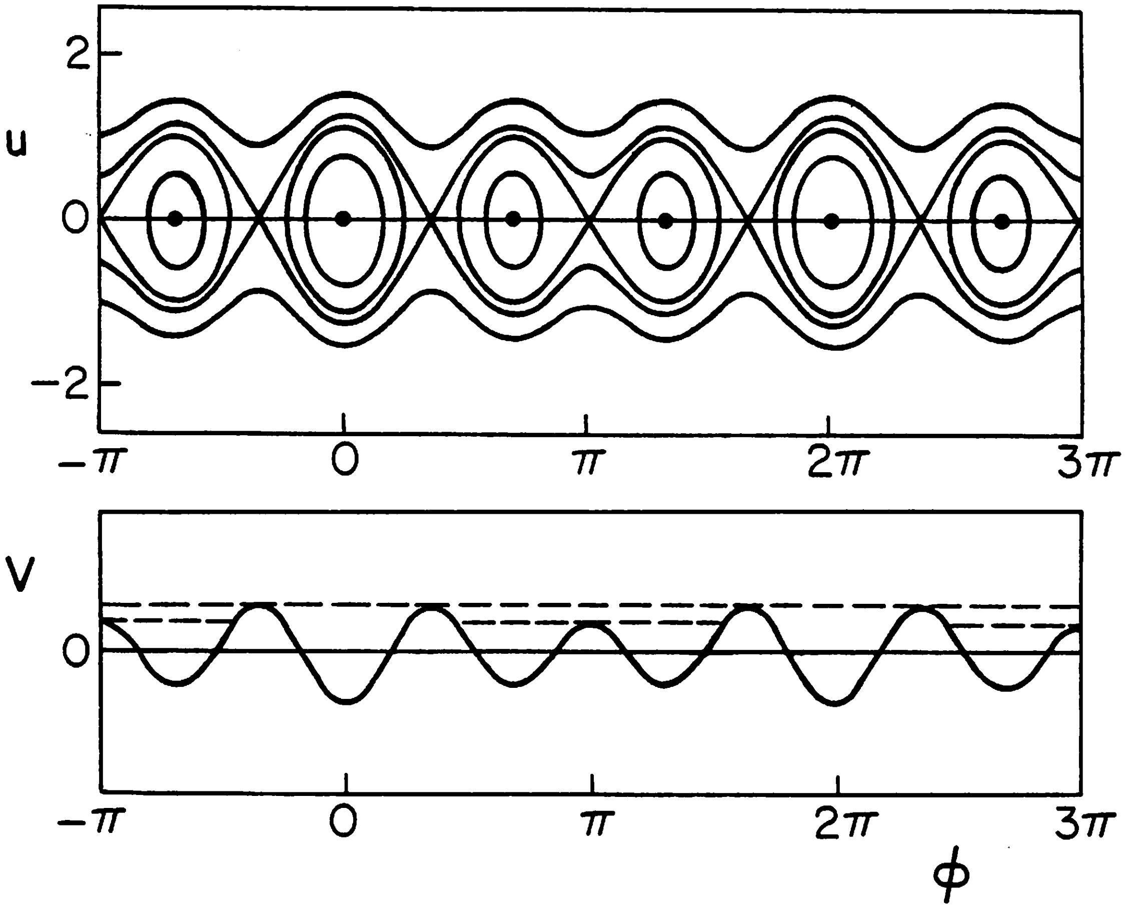

(d)

μ = 5

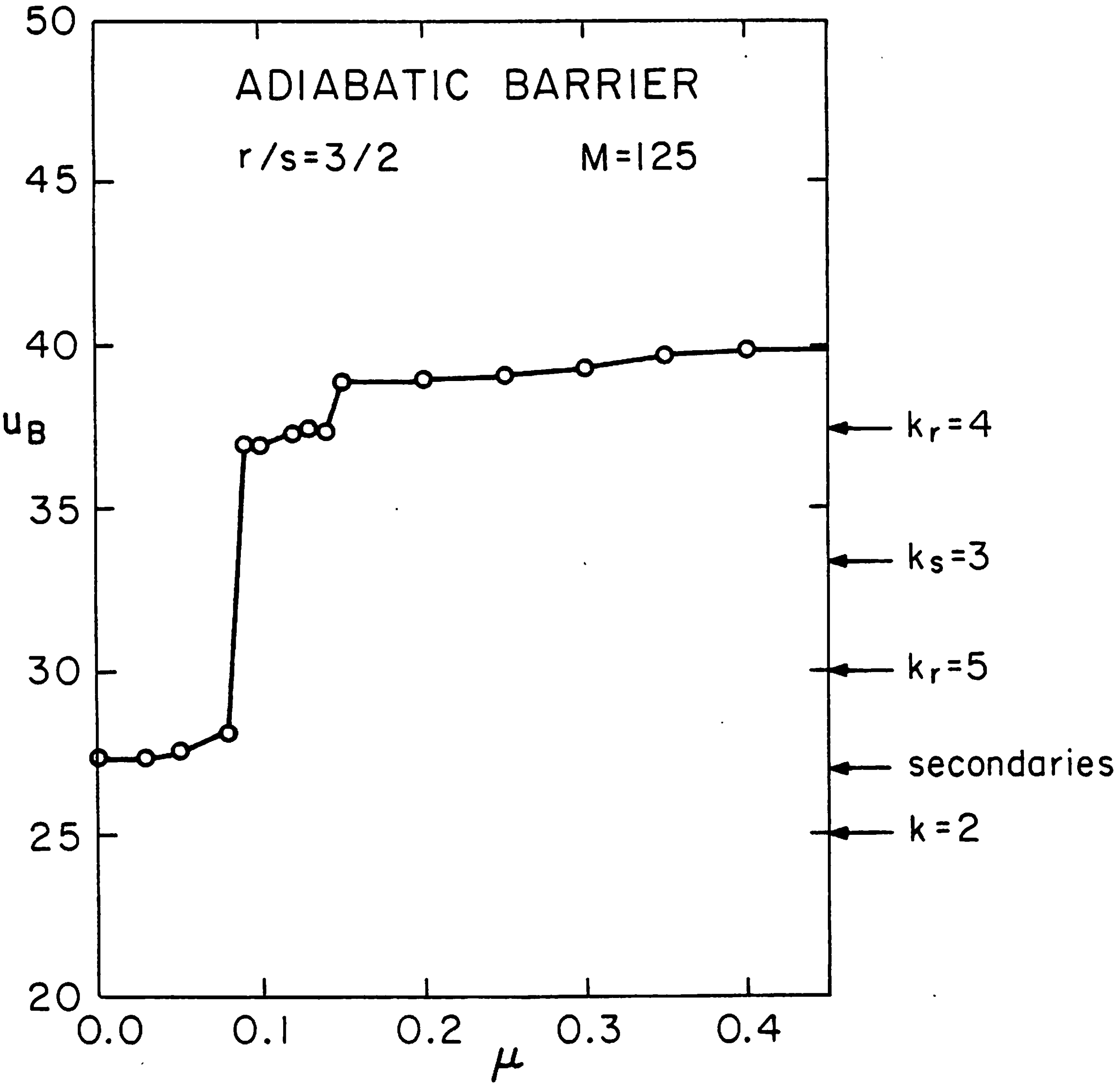
ADIABATIC BARRIER
r/s=3/2
M=125
u_B
50
45
40
35
30
25
20
0.0
0.1
0.2
0.3
0.4
μ
$k_r=4$
$k_s=3$
$k_r=5$
secondaries
$k=2$

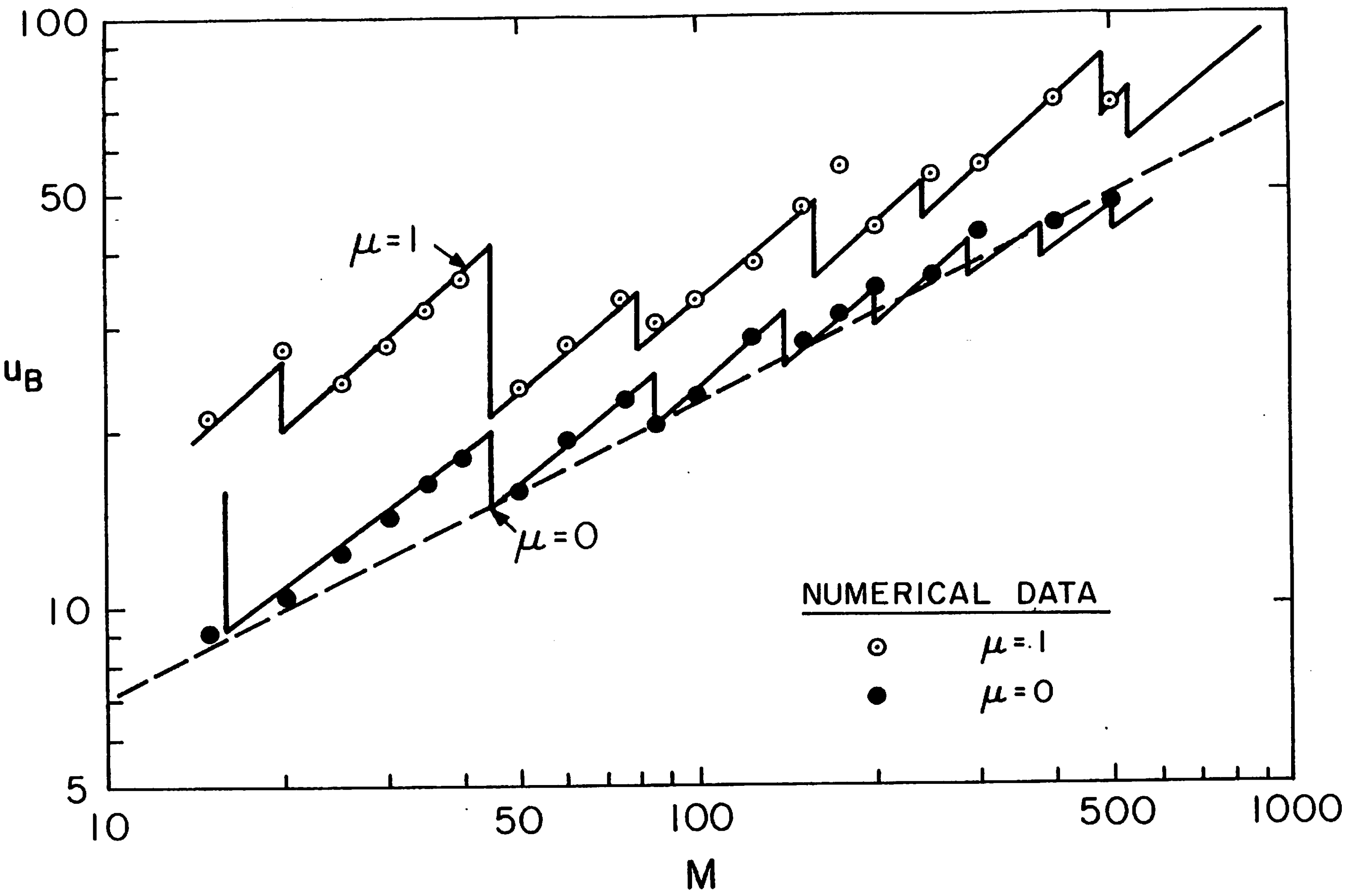
100
50
10
5
u_B
$\mu=1$
$\mu=0$
NUMERICAL DATA
⊙ $\mu=1$
● $\mu=0$
10
50
100
500
1000
M

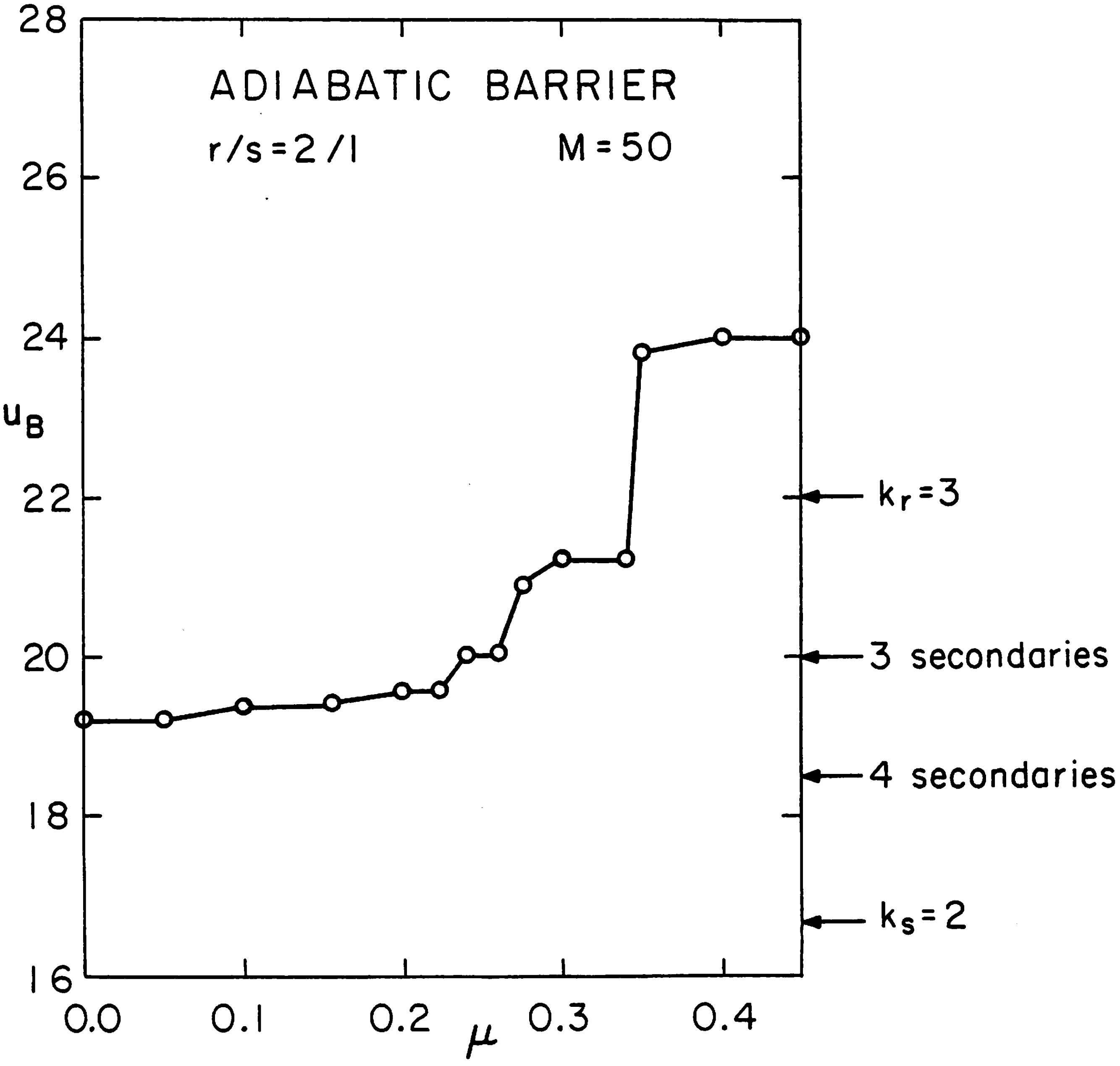

ADIABATIC BARRIER
r/s = 2/1
M = 50
u_B
28
26
24
22
20
18
16
0.0
0.1
0.2
0.3
0.4
μ
$k_r = 3$
3 secondaries
4 secondaries
$k_s = 2$

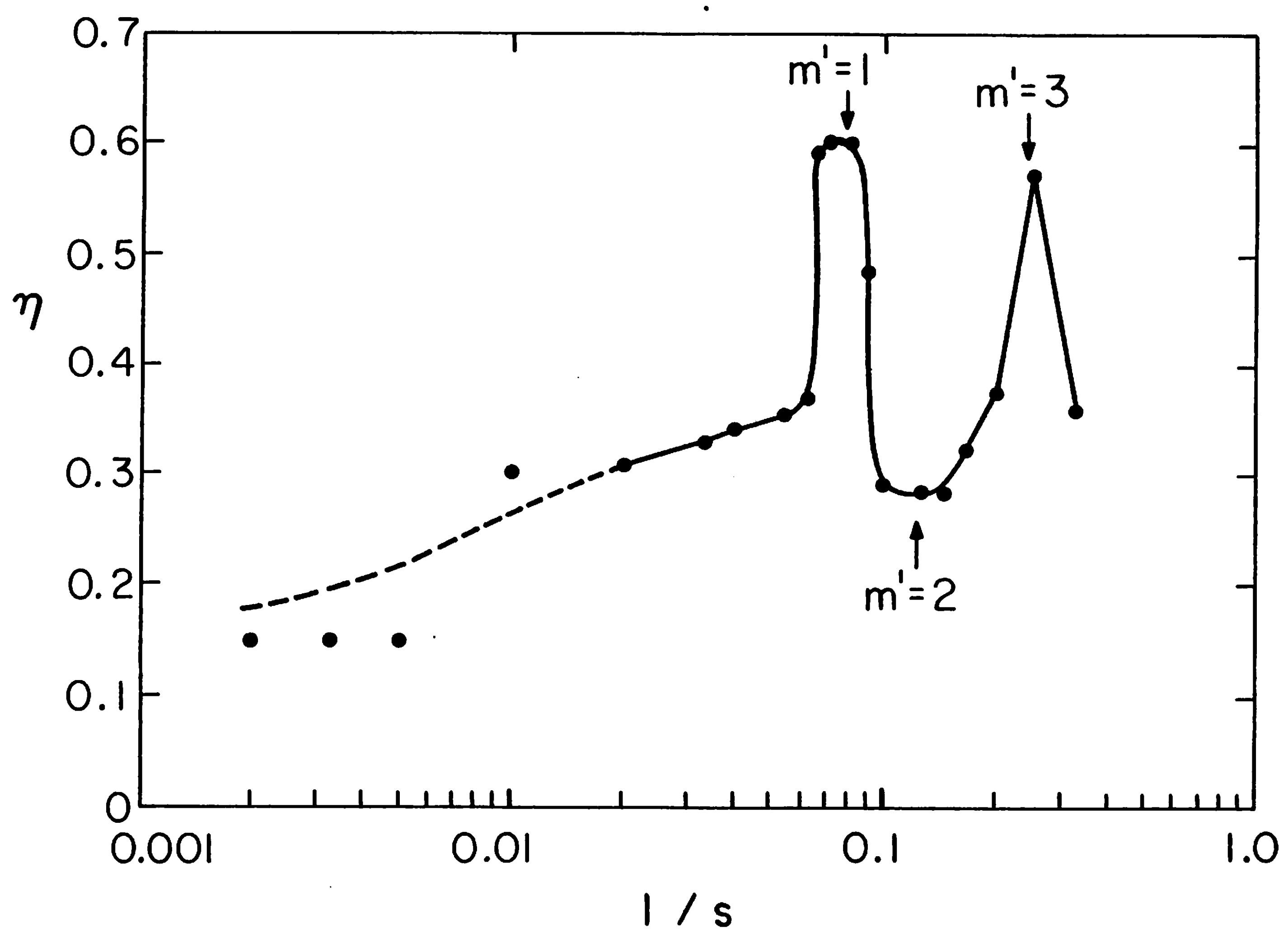
0.7
0.6
0.5
0.4
0.3
0.2
0.1
0
η
0.001
0.01
0.1
1.0
1 / s
m'=1
m'=2
m'=3